Biochimica et Biophysica Acta, 1184 (1994) 54–64

BBABIO 43965

Catalytic cooperativity in the Ca^{2+}-dependent ATPase activity of spinach chloroplast coupling factor (CF_1)

P. John Andralojc [1] and David A. Harris *

Department of Biochemistry, University of Oxford, South Parks Road, Oxford, OX1 3QU (UK)

(Received 1 April 1993)
(Revised manuscript received 28 July 1993)

Key words: Chloroplast coupling factor; ATPase, Ca^{2+}-; Unisite catalysis; Cooperativity; Alternating site; Data simulation

The Ca^{2+}-ATPase activity of CF_1, the soluble chloroplast coupling factor from spinach chloroplasts, was measured over ATP concentrations between 0.05 μM and 1000 μM. At very low ATP concentrations (< 1 μM), CF_1 exhibited a high affinity, low capacity mode of catalysis ($K_m = 0.05$ μM, $V_{max} = 1$ nmol min^{-1} mg^{-1}). This activity was unaffected by the ϵ-subunit of CF_1, and was stimulated 2–3-fold by tentoxin or by anti-CF_1 antibody. All three of these agents inhibit Ca^{2+}-ATPase at higher ATP concentrations. The pattern of ATP and ITP stimulation of $[^{32}P]P_i$ release from [γ-^{32}P]ATP, over the entire range of ATP concentrations studied, was investigated by mathematical modelling. Simulation of the observed data was possible only if three catalytic sites were operative, ruling out models for CF_1 turnover with only two catalytic sites for ATP hydrolysis (whether or not a solely regulatory site was also present). Cooperativity between catalytic sites was also required for simulation of the data. The resultant mathematical model for ATP hydrolysis can most simply be accommodated using a structural model for CF_1 in which three equivalent sites operate alternately during turnover (Boyer, P.D. (1989) FASEB J. 3, 2164–2178). We cannot, however, rule out a model in which an asymmetrical enzyme is maintained throughout turnover, providing that the catalytic sites in such an enzyme interact cooperatively during turnover.

Introduction

The H^+-ATP synthases constitute a group of homologous enzymes responsible for ATP synthesis, linked to H^+-translocation, in mitochondria, chloroplasts and bacteria. They comprise a membrane-spanning protonophore (F_0) and an ATPase assembly (F_1), bound to F_0 at the membrane surface. The F_1 component has a complex structure, with a subunit stoichiometry $\alpha_3\beta_3\gamma\delta\epsilon$ in which the three β subunits each bear a catalytic site (for reviews, see Refs. 1,2).

In mitochondrial F_1 (MF_1), the three catalytic ATP binding sites show decreasing affinities for ATP, the first ATP binding with very high affinity ($K_d \approx 10^{-12}$ M) [3–5] and the last with a much lower affinity ($K_m = 150$–250 μM) [6,7]. This indicates either (a) that the enzyme is initially asymmetrical, and the binding sites fill in order of affinity, or (b) that the enzyme is initially symmetrical, but shows negative cooperativity in binding. These alternative explanations have led to alternative models for catalysis, in which either (a) the asymmetrical catalytic sites have distinct functions (for example, one (or more) participating in ATP synthesis, while other(s) being specialised for hydrolysis [8]); or (b) all (essentially equivalent) sites participate in both synthesis and hydrolysis, each passing through equivalent conformations during turnover [6,7]. For a recent review, see Ref. 9. Similar models have been proposed to apply to CF_1, although the number of catalytic nucleotide binding sites on CF_1 is less well established [10].

Positive cooperativity in catalysis (stimulation of the turnover of substrate at low concentration by higher substrate concentrations) is demonstrable in F_1-ATPases from a variety of species [6,11–13]. Positive cooperativity cannot be explained on the basis of multiple asymmetric catalytic sites, and its operation is taken to support models with equivalent, interacting sites. We have previously demonstrated positive catalytic cooperativity during the Ca^{2+}-dependent hydrolysis of ATP by the soluble chloroplast F_1-ATPase (CF_1) [14]. We ruled out the possibility that the 'non-catalytic' nu-

* Corresponding author.
[1] Present address: Agricultural and Food Research Council, Institute of Arable Crops Research, Rothamsted Experimental Station, Harpenden, Herts., AL5 2JQ, UK.

Abbreviations: CF_1, MF_1, soluble coupling factor ATPase from chloroplasts, mitochondria; Tricine, *N*-[2-hydroxy-1,1-bis(hydroxymethyl)ethyl]glycine; IgG, immunoglobulin G.

SSDI 0005-2728(93)E0166-N

cleotide binding sites of CF_1 were involved in stimulation of catalysis, since ITP, which binds specifically to catalytic sites [15,16], also supported these effects.

Cooperative catalysis was dependent on the prior activation of CF_1 (which is a latent ATPase) either by removal of the ϵ subunit, or by exposure to dithiothreitol (DTT), or by the addition of ethanol to the assay medium. We also concluded that most of the activity manifest by native (predominantly ϵ-replete) CF_1 was due to traces of ϵ-depleted material in the preparation [14].

In the present work, a theoretical model was developed to probe catalytic cooperativity in CF_1. It is shown that the observed kinetics of ATP hydrolysis by CF_1 require the operation of three catalytic modes; two modes are insufficient. In other words, the two pairs of K_m and V_{max}values identified previously [14] must be supplemented by an additional (intermediate) K_m/V_{max} pair. Computer simulations based on this theoretical model allow the calculation of these intermediate values of K_m and V_{max}, which cannot otherwise be readily deduced. This work further confirms that the three catalytic sites of CF_1 interact cooperatively; models allowing all three sites to act independently cannot simulate the observed behaviour. It is also shown that anti-CF_1 antibodies and tentoxin (like azide [14]) inhibit CF_1 by abolishing cooperativity between catalytic sites, since they have an inhibitory effect on multisite, but not unisite, catalysis.

Methods

Materials and assays

Preparation of CF_1 and ϵ-depleted CF_1 was as described previously [17]. Both were frozen in liquid nitrogen and stored at −70°C. Dithiothreitol-activated CF_1 was prepared according to Patrie and McCarty [18]. Prior to assay of ATP hydrolysis, free ATP was removed from the coupling factor preparations by centrifugation through two consecutive Sephadex G-50 columns [19], equilibrated with 20 mM Tricine-NaOH (pH 8.0), 1 mM EDTA. Activated CF_1 contained 2 mol tightly bound ATP per mol CF_1. Tightly bound ADP (bound to a catalytic site on CF_1) was removed during CF_1 activation [42].

For treatment with tentoxin, ambient nucleotide was first removed from CF_1 (essentially as above), which was then diluted to 25 μg protein ml^{-1} in 20 mM Tricine-NaOH (pH 8.0) and incubated with 0.25 μM tentoxin for 60 min at room temperature [20]. Controls, lacking tentoxin, were prepared similarly. ATPase activity was then assayed immediately.

IgG was prepared from rabbits, before and after inoculation with pea or spinach CF_1, by standard procedures [21]. Immune and pre-immune IgG were incubated with 100 μl aliquots of desalted CF_1 in 20 mM Tricine-NaOH (pH 8.0). CF_1 concentration was 15 $\mu g\,ml^{-1}$ throughout, but IgG concentration varied between 15 and 750 $\mu g\,ml^{-1}$ (i.e., up to a 50-fold excess (w/w) of antibody). After 5 min at 37°C, aliquots were taken for ATPase assay.

ATP hydrolysis was assayed using [γ-^{32}P]ATP, as described in Ref. 14. The progress of hydrolysis was linear between 0 and 4 min [14], at all concentrations of ATP used. Concentration of CF_1 was measured by the dye-binding method of Bradford [22] using a proprietary reagent (Bio-Rad) and bovine serum albumin (BSA) as standard. IgG concentration was determined spectrophotometrically as described in Ref. 23. BSA, Tricine, and tentoxin were supplied by Sigma. [γ-^{32}P]ATP was supplied by Amersham. ATP and ITP were obtained from Boehringer-Mannheim. All other chemicals were obtained from British Drug Houses and were of analytical (AnalaR) grade. For the determination of K_m and V_{max} from initial velocity measurements, we used a non-linear regression analysis program (Enzfitter, from Elsevier-Biosoft).

Theoretical treatment

For any enzyme obeying Michaelis Menten kinetics, the fraction (L) of enzyme bound to ligand, is given by:

$$L = [S]/(K_m + [S]) \quad (1)$$

and the rate of reaction, ν, at constant enzyme concentration is given by

$$\nu = V_{max}[S]/(K_m + [S]) = V_{max}L \quad (2)$$

Consider an enzyme with several active sites (1, 2....n, in order of decreasing affinity for substrate), capable of conducting catalysis in distinct *modes*, each of which have distinct values of K_m and V_{max}. For non-interacting sites, the fraction of each class of site with bound ligand (L1, L2,...) will be given by:

$$L1 = [S]/(K_m1 + [S]),\ L2 = [S]/(K_m2 + [S])$$

etc., where K_m1 and K_m2 are the values of K_m for catalysis in mode 1 and mode 2, respectively.

However, if the sites interact in such a way that the second site can be filled only after the first (the *cooperativity* assumption) then the fraction of enzyme with two sites filled, $L2$, is now given by:

$$L2 = L1[S]/(K_m2 + [S]) \quad (3)$$

and similarly for the third site:

$$L3 = L2[S]/(K_m3 + [S])$$

The data of Boyer and co-workers [11,25] suggest that a single enzyme molecule can exhibit only one mode of catalysis at a time, i.e., that occupation of site

2 suppresses the operation of the highest affinity mode of catalysis (mode 1), and occupation of site 3 suppresses operation by modes 1 and 2. This refinement, which we call the *suppression* assumption, can also be incorporated into our model. In this case the contributions by modes 1, 2 and 3 to the overall rate of catalysis (denoted by $LV1$, $LV2$ and $LV3$, respectively) are given by:

$$LV1 = (L1 - L2)V_{max}1 \quad (4)$$

$$LV2 = (L2 - L3)V_{max}2 \quad (5)$$

$$LV3 = L3V_{max}3 \quad (6)$$

and the overall rate of catalysis, ν, for an enzyme with 3 catalytic sites is given by:

$$\nu = LV1 + LV2 + LV3 \quad (7)$$

Thus, if the three values of K_m and V_{max} are known, Eqn. 7 will allow the calculation of the overall reaction rate in such a cooperative system. Conversely, if ν is measured at a variety of [S], this equation can be used to calculate any K_m/V_{max} pair, if the other two pairs are known.

In previous experiments [14], our experimental parameter was not ν directly but Q, where

$$Q = \text{rate of } [^{32}P]P_i \text{ release at [ATP]/rate of } [^{32}P]P_i \text{ release at } [ATP]_L \quad (8)$$

where $[ATP]_L$ was a fixed, low concentration of ATP and [ATP] a variable concentration (such that $[ATP] > [ATP]_L$). In addition, we maintained the *total* radioactivity in [γ-^{32}P]ATP constant irrespective of ATP concentration. Under these conditions, Eqn. 7 can be used to predict values of Q, yielding the formula

$$Q = \nu \cdot [ATP]_L / \nu_L \cdot [ATP] \quad (9)$$

where ν and ν_L represent the rates at variable and low [ATP] respectively. (Note that, under these conditions, the specific radioactivity is inversely proportional to [ATP].)

Thus we can use Eqn. 9, together with 3 pairs of estimated K_m/V_{max} values to predict Q for any value of [ATP]. Comparison of the predicted values with the experimental values over a range of [ATP] will allow refinements of the estimates of K_m and V_{max} by curve fitting procedures, using the algorithm given in Appendix I.

A similar treatment can be used to predict the rate of ATP hydrolysis in the presence of ITP, except that (a) in this case, K_m from Eqn. 1 represents the apparent K_m for ATP, K_A, given by:

$$K_A = K_m(1 + \{[ITP]/K_I\})$$

where K_I represents the dissociation constant for ITP; and

(b) the fraction of enzyme with bound ligand, $L1$ (used in Eqn. 3) is the sum of the fraction bound to ATP ($H1$) and that bound to ITP ($I1$). Thus:

$$H1 + I1 = L1 = [ATP]/(K_A + [ATP]) + [ITP]/(K_I' + [ITP])$$

where K_I' represents the apparent affinity for ITP (in the presence of ATP).

In the treatment used initially (see Appendix II), it was also assumed that the relative affinities of ATP and ITP at each of the catalytic sites was constant, i.e.,

$$K_I1/K_m1 = K_I2/K_m2 = K_I3/K_m3 = R$$

where K_In represents K_d for ITP at the nth catalytic site. (This condition was relaxed in later simulations.)

A parameter $Q(I)$, analogous to Q above, is defined as

$$Q(I) = \text{rate of } [^{32}P]P_i \text{ release} + \text{ITP/rate of } [^{32}P]P_i \text{ release} - \text{ITP}.$$

Using the above parameters, the values of Q(I) can be predicted for all concentrations of ITP and ATP (see Appendix II).

Results

Direct estimation of K_m1 and K_m3

The Ca^{2+}-dependent ATPase activity of CF_1 was measured over a wide range of ATP concentrations (0.05 μM to 1000 μM). Estimates of K_m and V_{max} for CF_1 could be made by standard procedures; however, more than one value of K_m and V_{max} were required to describe the observed data. Thus, our preparation of CF_1 can carry out a high affinity, low capacity mode of turnover in addition to the more familiar high capacity, lower affinity mode [14].

Fig. 1 (A and B) illustrates the estimation of K_m and V_{max} values, using data at either end of this concentration range. Several determinations of this kind gave average values for K_m and V_{max} of 0.08 μM and 1 nmol min^{-1} mg^{-1} over the range 0.05 to 1 μM ATP; and of 390 μM and 5.9 μmol min^{-1} mg^{-1}, over the range 100 to 1000 μM ATP.

The experiment depicted in Fig. 1A uses non-activated (ϵ-replete) CF_1 for estimating K_m and V_{max} over the range 0.05–1 μM ATP, since in this preparation, lower affinity sites contribute little to total turnover [14], and estimation of activity at the high affinity site can be more precise. However, the values

obtained are identical (within experimental error) to those obtained for ϵ-depleted CF_1 (see below).

Properties of the high affinity mode of CF_1 turnover

We have previously shown that the high affinity, low capacity mode of ATPase activity in CF_1 preparations was unaffected by azide, or the CF_1-ϵ subunit. Both of these strongly inhibit the high capacity mode of turnover by CF_1 [14]. It was possible, therefore, that the high affinity mode of turnover observed might be due to a contaminating ATPase and be unrelated to CF_1 itself.

This possibility is eliminated by the experiments shown in Figs. 2 and 3, where the effects of CF_1 inhibitors tentoxin and anti-CF_1 antibody, respectively, are shown. Both of these reagents inhibit the high capacity mode of CF_1 turnover (measured at high ATP concentrations) but, remarkably, stimulate the low capacity (high affinity) mode. Since both reagents interact specifically with CF_1, the low capacity mode, too, must be an intrinsic property of this protein.

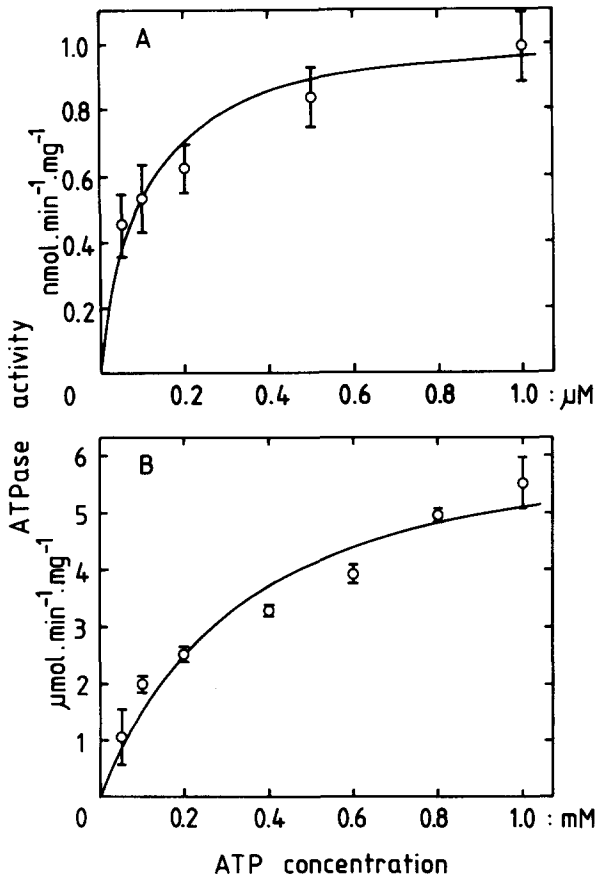

Fig. 1. Substrate dependence of Ca^{2+}-ATPase activity of CF_1. (A) ATPase activity of native (non-activated) CF_1, assayed at a concentration of 15 μg protein ml^{-1}. Error bars show range of 3 duplicate determinations. (B) ATPase activity of activated (ϵ-depleted) CF_1, assayed at a concentration of 1.5 μg protein ml^{-1}. A single (duplicate) determination is illustrated. The plotted curves were generated by non-linear regression.

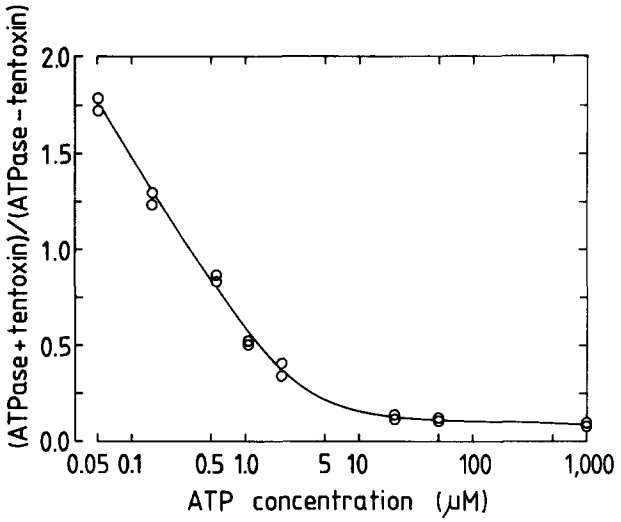

Fig. 2. Effects of tentoxin on 'high affinity mode' and 'low affinity mode' Ca^{2+}-ATPase. ϵ-depleted CF_1 was freed from ambient nucleotides, and incubated (25 μg protein ml^{-1}) with or without tentoxin (0.25 μM) as described in Methods. Ca^{2+}-ATPase activity was then determined at various ATP concentrations. Results are expressed as (rate + tentoxin)/(rate − tentoxin) at each ATP concentration.

Fig. 2 shows the effect of a low concentration of tentoxin (0.25 μM) on ATPase activity by ϵ-depleted CF_1 over a wide range of ATP concentrations. At high concentrations of ATP (> 25 μM), when the high capacity mode predominates, tentoxin inhibits Ca^{2+}-ATPase by more than 90%. At low concentrations of ATP (< 0.1 μM), however, when the low capacity mode predominates, ATPase is stimulated up to 2-fold. Tentoxin had a similar effect on dithiothreitol-activated CF_1 (data not shown).

It has been reported [25] that high concentrations of tentoxin can also stimulate the high capacity mode of CF_1 turnover. However, these experiments were performed at concentrations of tentoxin over 100-fold higher than those used in our experiments. As can be seen from Fig. 2, tentoxin strongly inhibits the high-capacity mode of turnover under the conditions used here.

Fig. 3 shows a similar experiment carried out with anti-CF_1 antibody, except that in this case Ca-ATP levels were fixed at 0.05 μM (high affinity mode) or 50 μM (high capacity mode), and the antibody concentration was varied. Again, the high capacity mode is strongly inhibited (up to 95% at antibody to CF_1 ratios of above 25:1 (w/w)) while the high affinity mode is stimulated up to 3-fold.

The IgG used in the experiment of Fig. 3 contained polyclonal antibodies against pea CF_1, but cross-reacted strongly with the spinach CF_1 used here. When the experiment was repeated using antibodies raised against spinach CF_1, the pattern of effects was somewhat different; the inhibitory effect on the high capac-

ity mode of turnover was retained, but no effect was observed on the low capacity mode (data not shown). This indicates that inhibition and activation may be due to different populations of antibody, interacting with different regions of CF_1. This conclusion is supported by consideration of the $c_{0.5}$ values for the two effects calculated from Fig. 3 – activation requires about twice as much antibody (7:1 (w/w) for 50% effect) as activation (4:1, w/w).

Thus, tentoxin and anti-CF_1 antibody join other reagents, such as azide and the ϵ-subunit of CF_1 [14], having differential effects on the high capacity and high affinity modes of CF_1 turnover. Relevant to the present work, however, their effects allow us to conclude with certainty that the high affinity, low capacity mode of turnover is a property of CF_1, since it is stimulated by reagents which interact specifically with CF_1.

Cooperativity in CF_1

Ca^{2+}-dependent ATP hydrolysis by CF_1 can be measured, using [γ-^{32}P]ATP, keeping the total amount of radioactive ATP constant in each assay, while varying the concentration of non-radioactive ATP. This approach is convenient for detecting positive cooperativity in catalysis, since if co-operativity is present, the amount of $[^{32}P]P_i$ liberated at one ATP concentration can exceed that at a lower concentration. Without promotion of catalysis by cooperativity, liberation of $[^{32}P]P_i$ from ATP must fall due to the decrease in its specific radioactivity [14,26].

Fig. 4 shows the variation in $[^{32}P]P_i$ release when ϵ-depleted CF_1 is exposed to increasing Ca-ATP concentrations. Rates are expressed as the relative rate of $[^{32}P]P_i$ release (Q) where

$$Q = \frac{\text{rate of } [^{32}P]P_i \text{ release at [ATP]}}{\text{rate of } [^{32}P]P_i \text{ release at a fixed low [ATP]}}$$

as defined in the theoretical treatment (Eqn. 8). Three phases are observed (Fig. 4, data points). Initially ([ATP] < 1 μM) the relative rate of $[^{32}P]P_i$ release falls to a trough, as would be expected from dilution of the specific radioactivity of ATP (Fig. 4, inset). However, Q then rises to reach a peak of maximum stimulation of over 3-fold at around 30–40 μM ATP. This indicates positive cooperativity between ATP binding sites on the protein. Finally, the relative rate falls away as [ATP] rises further and the specific radioactivity falls further.

Attempts were made to fit the observed data to a smooth curve, using the two K_m and V_{max} values obtained in Fig. 1, and the theoretical treatment above. Two points became clear immediately. First, as noted above, an assumption of independent sites would not fit the data; the predicted level of $[^{32}P]P_i$ release would decline continuously (broken line, Fig. 4). Secondly, the data could not be fitted if only two nucleotide binding sites were present; in this case, whatever K_m/V_{max} pairs were taken, it was impossible to simulate both a trough and a peak in the data curve [27].

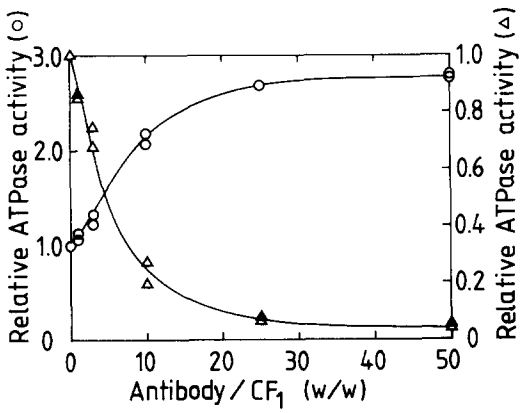

Fig. 3. Effects of anti-CF_1 antibody on 'high affinity mode' and 'low affinity mode' Ca^{2+}-ATPase. CF_1 was freed from ambient nucleotides, and incubated with varying amounts of IgG (as indicated) as described in Methods. ATP hydrolysis was then determined at [ATP] = 0.05 μM, using native CF_1 (○), and [ATP] = 50 μM using ϵ-depleted CF_1 (△). Rates are expressed as (rate + anti-CF_1)/(rate + pre-immune IgG) at each IgG concentration. A relative ATPase activity of 1 corresponds to a rate of 0.15nmol $min^{-1}mg^{-1}$ at 0.05 μM ATP and 1.15 μmol $min^{-1}mg^{-1}$ at 50 μM ATP.

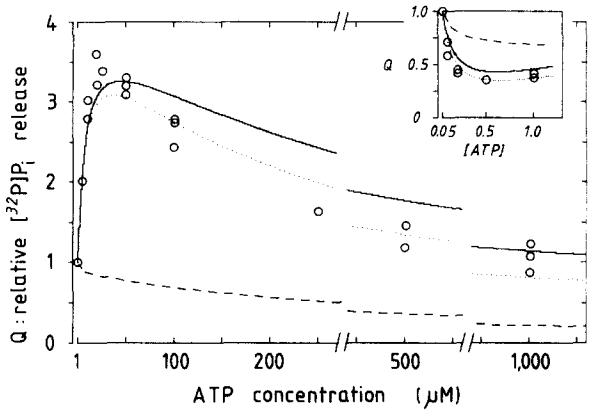

Fig. 4. Observed and predicted hydrolysis of [γ-^{32}P]ATP. $[^{32}P]P_i$ release from [γ^{32}P]ATP was measured as described under Methods, using 1.5 μg/ml ϵ-depleted CF_1. Radioactivity was fixed at 0.4 μCi/ml. For the inset data (range 0.05–1 μM ATP), the rate (Q) was expressed relative to that at 0.05 μM, whereas for the main figure (1–1000 μM), Q was expressed relative to that at 1 μM ATP. Open circles represent experimental values.The illustrated curves represent predicted values of Q with (i) K_m and V_{max} for modes 1 and 3 as determined in Fig. 1, and $K_m2 = 6$ μM and $V_{max}2 = 7$ nmol $min^{-1}mg^{-1}$ (solid line); (ii) as in (i), but omitting cooperativity assumption (broken line); (iii) values of K_m and V_{max} for modes 1 and 3 adjusted to optimise fit ($K_m1 = 0.05$ μM, $V_{max}1 = 1.0$ nmol $min^{-1}mg^{-1}$, $K_m3 = 250$ μM, $V_{max}3 = 4.0$ μmol $min^{-1}mg^{-1}$, dotted line). For simulations, see theoretical section.

Thus, fitting the data required the assumption of three interacting nucleotide binding sites on the enzyme. The third site required K_m/V_{max} values between the low values of Fig. 1A and the high values of Fig. 1B. We designate these three sites as 1, 2 and 3, in order of decreasing affinity.

Using curve fitting procedures, our model was now used to estimate values for this intermediate K_m/V_{max} pair (K_m2 and $V_{max}2$). First, we fixed K_m1, $V_{max}1$ at the values calculated from Fig. 1A, and found values of K_m2 and $V_{max}2$ which best fitted the inset data in Fig. 4 (within the solid lines, Fig. 5). Next we fixed K_m3, $V_{max}3$ at the values calculated from Fig. 1B, and found values of K_m2 and $V_{max}2$ which best fitted the remaining data in Fig. 4 (within the dashed lines, Fig. 5). Values of K_m2 and $V_{max}2$ applicable over the entire range of data must therefore lie within the (overlapping) shaded region (K_m between 4 and 20 μM, V_{max} between 2 and 40 nmol min^{-1} mg^{-1}). Values of K_m2 greater than 12 μM were eliminated since they gave a position for the peak of Q at greater than 65 μM Ca-ATP (dotted line, Fig. 4), which is incompatible with the data in Fig. 4.

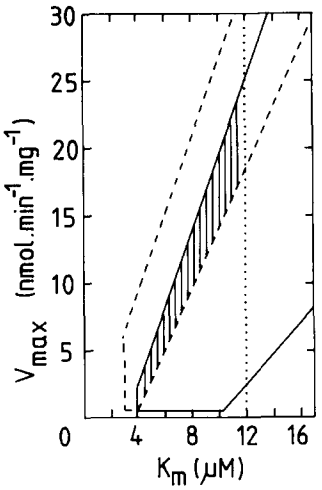

Fig. 5. Defining K_m and V_{max} for catalysis in mode 2. The values for K_m3 and $V_{max}3$ were taken from Fig. 1B, and simulations of the data in Fig. 4 (main figure) were performed, using a matrix of values for K_m2 and $V_{max}2$ varying by 0.5 μM and 0.5 nmol min^{-1} mg^{-1} respectively. Acceptable combinations (within the broken line) were defined as those with the peak of Q between 20–55 μM and of a height between 2.8 and 3.3. As shown in Appendix I and Ref. 27, raising K_m2 moves the peak to the right and raising $V_{max}2$ leads to a fall in peak height. For example, values for K_m2 above 12 μM (dotted line) place the position of the peak of $[^{32}P]P_i$ release above 65 μM ATP. Simulations of the inset data were performed using the values of K_m1 and $V_{max}1$ from Fig. 1A, and the same range of values for K_m2 and $V_{max}2$. Hence, the *overlap* (shaded) region contains combinations of K_m2 and $V_{max}2$ which yield curves of Q versus ATP concentration, in fair agreement with experimental data over the entire ATP concentration range; optimal values (see Fig. 4) were then determined by linear regression.

TABLE I

Kinetic parameters of ATP hydrolysis by CF_1

Parameters for the three modes of catalysis which generated the curves shown in Fig. 4, according to the model given under Theoretical treatment (see text). **A**: Parameters for modes 1 and 3 determined from Fig. 1, and for mode 2 estimated from Fig. 4. **B**: Parameters for modes 1 and 3 optimised by fitting data in Fig. 4.

	Mode 1	Mode 2	Mode 3
A.			
K_m (μM)	0.08	6	390
V_{max} (nmol min^{-1} mg^{-1})	1.0	7	5900
B.			
K_m (μM)	0.05	6	250
V_{max} (nmol min^{-1} mg^{-1})	1.0	7	4000

Values of K_m2 and $V_{max}2$ were then optimised by choosing those values which gave best fits for the positions of the peak and trough (where $dQ/d[ATP] = 0$). The values obtained for K_m2 and $V_{max}2$ were 6 μM and 7 nmol min^{-1} mg^{-1}, respectively. These three K_m/V_{max} pairs (Table IA) were then used to simulate the variation in Q over the entire range of ATP concentrations, resulting in the solid curve shown in Fig. 4. Subsequent small changes in the values for K_m1, $V_{max}1$, K_m3 and $V_{max}3$ were found to improve the fit between predicted and observed data (Fig. 4, dotted line). The best fit was observed at the values shown in Table IB, and these are considered to be the likely values for the three sites.

As mentioned above, it is important to know how the simulated curves change when the 'cooperativity assumption' is omitted from the calculations (see above). The broken line in Fig. 4 shows, in fact, the predicted variation in Q with [ATP] for a three-site model with the K_m and V_{max} values of Table IA in the absence of cooperativity.

These data were derived from studies on ϵ-depleted (i.e., activated) CF_1. However, this model will also simulate the behaviour of native (ϵ-replete) CF_1 (with a specific activity of around one-fiftieth the value for the activated preparation), and of dithiothreitol-activated CF_1, over a wide range of ATP concentrations [27], assuming that the ϵ subunit inhibits turnover in modes 2 and 3, as previously postulated [14]. This suggests that this model is generally valid for explaining Ca^{2+}-ATPase turnover by CF_1.

ATP hydrolysis in the presence of ITP

Since cooperativity involves interaction between the active sites of CF_1, analogues of ATP – such as ITP – will also stimulate ATP hydrolysis, under certain conditions [28,29]. Indeed, since the non-catalytic sites of CF_1 bind ITP poorly, if at all [15,16], observation of this stimulation is a good indication that we are dealing

solely with active site–active site interactions. Fig. 6 (upper data points) shows that, at a constant, low concentration of [γ-^{32}P]ATP (here 1 μM), ITP indeed has a considerable stimulatory effect on ATP hydrolysis, while at a higher ATP concentration (here 50 μM), a small inhibitory effect is observed (Fig. 6, lower points), which would be expected in the presence of a competing substrate in the absence of cooperativity.

For fitting these data to our simulations, knowledge of the three K_i values for ITP (for each of three nucleotide binding sites) was required. For convenience, we measured K_I3, the highest of the three values; K_I1 and K_I2 were then estimated by assuming a constant ratio, R, between K_m(ATP) and K_i(ITP) at each of the three sites (see Theoretical treatment). Assuming ITP to be a competitive inhibitor of ATPase activity, K_I3 was measured from inhibition experiments at [ATP] > 50 μM, as shown in Fig. 7. The value of K_I3 measured in this experiment was 5.2 ± 0.7 mM, giving an R value of $5.2/0.39 = 13$ (see Table IA).

On a plot of s/v versus s (Hanes plot) such as Fig. 7, it would be expected that varying concentrations of a competitive inhibitor would yield parallel lines. In fact, the lines of best fit (shown) depart slightly from parallel. This departure is probably within experimental error; alternatively it may reflect a slight tendency for ITP, at high concentration, also to replace ATP at 'non-catalytic' sites on the enzyme (see Ref. 30). However, Fig. 7 shows that this tendency is slight, even at very high ITP concentrations.

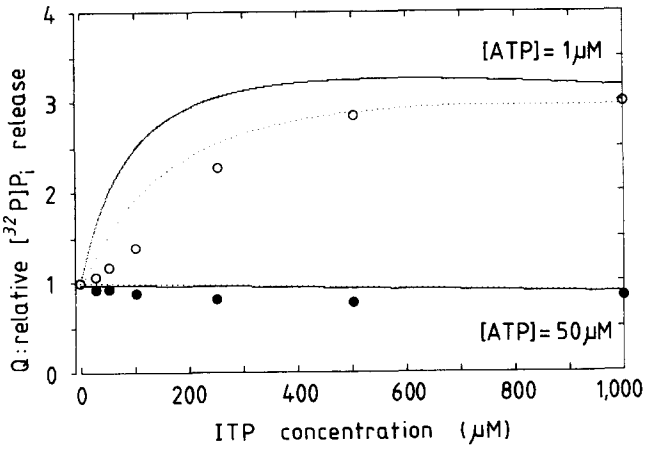

Fig. 6. Stimulation of ATP hydrolysis by ITP. [^{32}P]P_i release from ATP was assayed as in Fig. 4, in the presence of either 1 μM ATP (○) or 50 μM ATP (●), except that ITP was added to the assay as indicated. CF_1 concentration in the assay was 1.5 μg ml^{-1}. Symbols represent experimental values of $Q(I) = (\text{rate} + \text{ITP})/(\text{rate} - \text{ITP})$ (see Theoretical treatment). Curves illustrate the predicted values of $Q(I)$, with the values of K_m and V_{max} as in Table IA, and K_I3 as calculated from Fig. 7. Solid lines: R value (see text) set at 13 for each mode of catalysis. Dotted line: R value of 13 for modes 1 and 3, but 26 for mode 2.

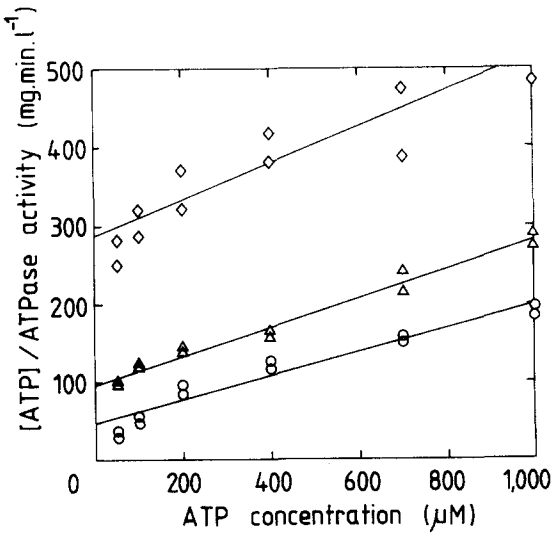

Fig. 7. Effect of ITP on ATP hydrolysis by CF_1 at high ATP concentrations. Ca ATP hydrolysis by ϵ-depleted CF_1 were measured as in Fig. 1, except that 0 mM (○), 10 mM (△), or 20 mM Ca-ITP (◇) was present as indicated. Plots are displayed according to Hanes. Estimates of K_m, V_{max} and K_I were obtained by curve fitting to a hyperbola using non-linear regression analysis.

Attempts were then made to simulate the data given in Fig. 6 assuming the K_m/V_{max} values given in Table IA, the measured value for K_I3 and a constant ratio $R = 13$ between K_m(ATP) and K_i at each of the three sites (see above). These values predict qualitatively the behaviour shown in Fig. 6 – a stimulation of the hydrolysis of 1 μM ATP at ITP concentrations between 50 μM and 1000 μM, and an inhibition of the hydrolysis of 50 μM ATP over the same range (Fig. 6, solid curves). A better fit to the data was obtained by relaxing the condition that R should be equal at all three sites; the dotted curves (Fig. 6) represent the predicted observations when R was allowed to rise 2-fold ($R = 26$) for site 2 only. No attempts were made to further optimise the fit by allowing three independent values of R.

Discussion

Unisite catalysis by CF_1

The work reported above confirms that our CF_1 preparation has a low capacity, high affinity mode of turnover, as reported previously [13]. The kinetic parameters of this mode of turnover are $V_{max} = 1.0 \pm 0.1$ nmol min^{-1}(mg protein)$^{-1}$ and $K_m = 0.08 \pm 0.03$ μM (Fig. 1A). This activity is stimulated by specific effectors of CF_1, anti-CF_1 antibody and tentoxin, showing that this activity is a property of CF_1 itself, and not of a trace contaminant.

CF_1 contains three catalytic sites per molecule. We interpret this low capacity mode of turnover as 'unisite

catalysis' – catalysis with only one of the three catalytic sites occupied. Unisite catalysis has also been reported to occur in CF_0CF_1 incorporated into liposomes [31,32], at a rate of 1.4 nmol min^{-1}(mg protein)$^{-1}$, almost identical to that measured here. It thus appears that unisite catalysis occurs in both free and membrane-bound F_1, and is not an artefact of F_1 isolation. Similar rates of catalysis (0.80 nmol min^{-1}(mg protein)$^{-1}$) have been recorded for ATP hydrolysis by the isolated β-subunit of CF_1 [33], where of course no cooperativity is possible, and catalysis must proceed via a 'unisite' mechanism. Unisite catalysis has also been recorded in F_1 from bovine heart and *E. coli* [3,34], showing that it is a common feature of F_1 across various species.

Unisite catalysis by various F_1 species is insensitive to the classical F_1 inhibitor, azide [26,35]. We have also shown it to be unaffected by the inhibitory (ϵ) subunit of CF_1 [14], and by anti-CF_1 antibody (above). Above, we show that, remarkably, this activity is stimulated (in spinach CF_1) by tentoxin and by anti-pea CF_1 at concentrations which nearly abolish the high capacity, low affinity ('multisite') catalysis (Figs. 2, 3). This indicates that these reagents abolish intersubunit cooperativity in F_1 but may actually increase the rate of product release from an individual active site – possibly by distorting a subunit interface. Similar effects have been seen in the $\alpha\beta$ 'core complex' of CF_1; turnover by this complex (which we consider as occurring in a unisite mode [36]) is insensitive to azide but stimulated by tentoxin [37]. Al-Shawi et al. [38] have also reported that antibodies raised against the β-subunit of EF_1 will inhibit azide-sensitive (multisite) hydrolysis by holo F_1 but will stimulate (unisite) catalysis by the isolated β-subunit.

All three catalytic sites of CF_1 participate in ATP hydrolysis

Analysis of the kinetics of Ca-ATP hydrolysis by CF_1 previously led us to the conclusion that at least two of the catalytic sites of CF_1 must participate in cooperative ATP hydrolysis [14]. Application of the quantitative treatment developed above to the data of Fig. 4 shows that three ATP binding sites must participate in catalysis. In particular, the pattern in [^{32}P]P_i release (at constant radioactivity) of a fall, followed by a rise and a second fall cannot be explained if only two catalytic sites are operating. This rules out models of F_1 function in which two catalytic sites participate in ATP hydrolysis [9,31], with the third possibly carrying out ATP synthesis.

As is shown in Fig. 4, successful simulation of the experimental data also requires a strict order of nucleotide binding to the catalytic sites, as opposed to simultaneous binding of ATP to all three sites dependent only on their relative affinities. This indicates cooperativity between the binding sites, as expressed in our 'cooperativity assumption' (see Theoretical treatment).

It should be noted that our data simulation also rules out the possibility of two catalytic sites and a 'regulatory' nucleotide binding site, since no peak is obtained in Fig. 4 unless all three sites are catalytically active, even if $V_{max}1$ and $V_{max}2$ are allowed to rise on filling a third site (data not shown).

Our calculated values for V_{max} for Ca-ATP hydrolysis by CF_1 (Table I) provide estimates of the k_{cat} values for each mode of catalysis, of 0.007 s^{-1}, 0.05 s^{-1} and 40 s^{-1} (assuming mol. mass of CF_1 = 400 kDa). This is in good agreement with values reported by Fromme and Graber for turnover by CF_0F_1 (0.009 s^{-1}, 0.5 s^{-1} and 80 s^{-1}), measured by a different technique [31]. The largest deviation, between the two values for $k_{cat}2$, may reflect the greater uncertainty on this value (Fig. 5) compared to the other two values or, possibly, some quantitative differences in the kinetics of membrane bound and free CF_1.

Are all three catalytic sites equivalent?

The successful prediction of the unusual kinetic behaviour of CF_1 (a) over a wide range of ATP concentrations (Fig. 4), (b) in the presence and absence of ITP (Fig. 6), and (c) for ϵ-depleted and ϵ-containing CF_1 (data not shown), suggests that our three-site cooperative model for nucleotide hydrolysis by CF_1 is likely to be correct. The ability of ITP to participate in cooperative hydrolysis makes it unlikely that cooperation involves 'non-catalytic' nucleotide binding sites in CF_1, since these have a high specificity for adenine nucleotide. Furthermore, this mechanism shows a similarity between the Ca^{2+}-ATPase of CF_1 and the Mg-ATPase of MF_1, whereas it has been suggested that Ca^{2+}-ATPase activity might operate by an inherently different mechanism.

Our theoretical treatment is based on a model of F_1 turnover proposed by Boyer and co-workers, in which three intrinsically equivalent catalytic sites pass through identical conformations, albeit 120° out of phase [39]. In other words, although F_1 may appear asymmetrical at any instant, the sites are symmetrically organised over a time averaged turnover. Scheme I shows how three values for K_m and V_{max} could arise in such a system, through unisite, 'bisite' and trisite modes of catalysis. (Note that the need to retain asymmetry leads to a rather complex model for catalysis in which only two catalytic binding sites fill during turnover – so-called 'bisite' catalysis.)

Our foregoing analysis and data fitting cannot, however, rule out alternative ('asymmetrical') models in which one nucleotide binding site is permanently different from the others. It does, however, place very specific restrictions on such models: three (not two) catalytic sites must participate in hydrolysis, and bind-

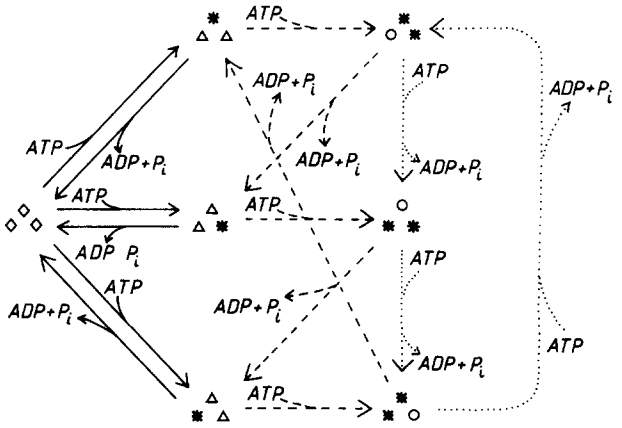

Scheme I. Possible conformations of CF_1 during ATPase turnover.The scheme is based on a model of CF_1 turnover in which all three catalytic sites are equivalent (see text). *: adenine nucleotide bound at a catalytic site; ◇: high affinity conformation; △: intermediate affinity conformation; ○: low affinity conformation (all unoccupied); —: turnover at unisite rate (mode 1); - - -: turnover at bisite rate (mode 2); ...: turnover at trisite rate (mode 3).

ing to the looser site(s) must stimulate catalysis at (at lease one of) the tighter. Extant models involving the asymmetrical operation of F_1 [8,32,40,41] do not specify these conditions.

On balance, therefore, the success of our theoretical model in fitting the observed data (Figs. 4 and 6) suggests that CF_1 turnover occurs by an alternating sites mechanism, with three equivalent catalytic sites, as has been proposed for MF_1 by Boyer and co-workers [11,39] and supported by their isotope exchange data [12,24]. Additional support for site equivalence from the present work is the observation that the relative affinities for ITP and ATP (the ratio R, above) appear to be similar at each catalytic site (Fig. 6), whereas an asymmetrical model might predict large differences in affinity. Clearly, no kinetic analysis can rule out all possible asymmetric models for ATP hydrolysis by CF_1; however, restrictions placed on such models by our analysis restricts the types of reaction mechanism suitable for consideration.

Acknowledgements

Financial support for the initial stages of this work was provided by the Agricultural and Food Research Council (grant no. AG 43/139). We also thank the Science and Engineering Research Council for support.

Appendix I. Simplified algorithm for determination of Q

Although the program below is written in BASIC, it can easily be modified for use with a spreadsheet. The symbols used are as described under Theoretical treatment, except that the components of the calculation at the higher ATP concentration are prefixed by 'H' (instead of 'L', which is reserved for the lowest, reference, concentration). This algorithm applies to both ranges of ATP concentration, shown in Fig. 4. For clarity, details relating to graphical representation of the data have been omitted, the results simply being stored in a 2-dimensional array: $V([ATP],Q)$. Values for K_m1, $V_{max}1$, K_m3 and $V_{max}3$ were from Table IA. As written, K_m2 and $V_{max}2$ may be varied, and the effect on Q evaluated. Fig. 8 (A and B) shows the effect of different $V_{max}2$ and K_m2 values, respectively, on the ATP dependence of Q.

Appendix II. Hydrolysis of ATP in the presence of ITP

ITP can be regarded as a competitive inhibitor of ATP hydrolysis by CF_1. Thus, in the presence of ATP, the apparent K_m for ATP, K_A is given by

$$K_A = K_m(1+[ITP]/K_I) \quad (10)$$

where K_m is the true K_m for ATP and K_I is the

```
10  REM DEFINE KM AND VMAX VALUES
20  LET KM1=.08:LET V1=.001
30  INPUT "INITIAL KM2 ";INITKM2
40  INPUT "FINAL KM2 ";FINKM2
50  INPUT "INCREMENT ";INCKM2
60  INPUT "INITIAL VMAX2 ";INITV2
70  INPUT "FINAL VMAX2 ";FINV2
80  INPUT "INCREMENT ";INCV2
90  LET KM3=390:LET V3=5.9
100 REM SET INITIAL (X),FINAL (Y) AND
110 REM INCREMENT (Z) IN [ATP]
120 LET X=1:    REM OR X=.05
130 LET Y=1000: REM OR X=1.00
140 LET Z=2.5:  REM OR Z=.01
150 LET W=(Y/Z)+1:DIM V(W,2)
160 REM CALCULATING Q FOR EACH [ATP]
170 REM (AT SELECTED VALUES OF KM2 AND V2)
180 FOR K2=INITK2 TO FINK2 STEP INCK2
190 FOR V2=INITV2 TO FINV2 STEP INCV2
200 LET L1=X/(X+KM1)
210 LET L2=(L1*X)/(X+KM2)
220 LET L3=(L2*X)/(X+KM3)
230 LET LV1=(L1-L2)*V1
240 LET LV2=(L2-L3)*V2
250 LET LV3=L3*V3
260 LET LV=LV1+LV2+LV3
270 FOR C=1 TO W
280 LET N=X+(C*Z-Z)
290 LET H1=N/(N+KM1)
300 LET H2=(H1*N)/(N+KM2)
310 LET H3=(H2*N)/(N+KM3)
320 LET HV1=(H1-H2)*V1
330 LET HV2=(H2-H3)*V2
340 LET HV3=H3*V3
350 LET HV=HV1+HV2+HV3
360 LET Q=(HV*X)/(LV*N)
370 LET V(C,1)=N: LET V(C,2)=Q
380 NEXT C
390 NEXT V2
400 NEXT KM2
410 STOP
```

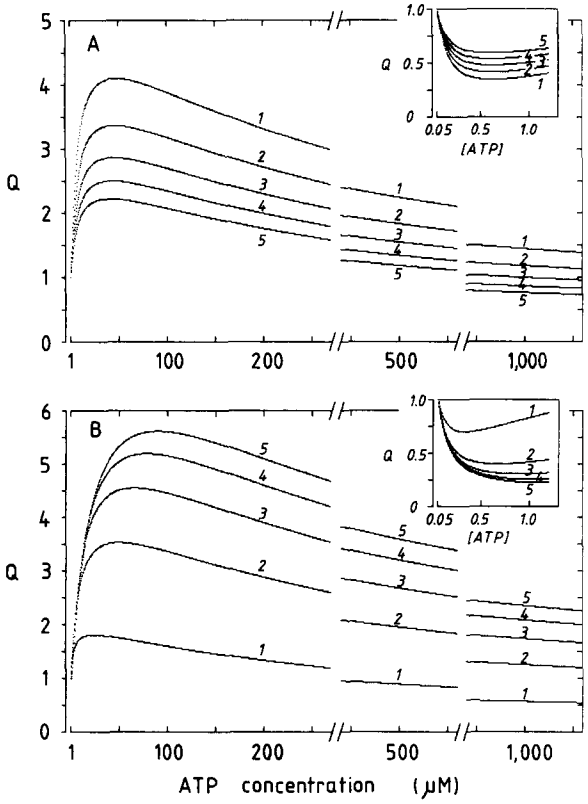

Fig. 8. Effect of varying $V_{max}2$ and K_m2 on the predicted variation of Q with ATP concentration. Q was calculated as in the Theoretical treatment, using the values of $V_{max}1$, K_m1, $V_{max}3$ and K_m3 derived from Fig. 1. Insets show the range from 0.05 μM to 1 μM ATP. (A) $K_m2 = 6$ μM; $V_{max}2 =$ (1) 1; (2) 6; (3) 11; (4) 16; (5) 21 nmol $min^{-1} mg^{-1}$. (B) $V_{max}2 = 7$ nmol $min^{-1} mg^{-1}$; $K_m2 =$ (1) 2; (2) 7; (3) 12; (4) 17; (5) 22 μM.

dissociation constant for ITP. CF_1 can hydrolyse ATP in one of three distinct modes, each mode characterised by a distinct value of K_m and V_{max}. Since K_I for each of these three modes is not known, the additional simplifying assumption is made that, for the nth mode of catalysis:

$$K_I(n) = R \cdot \{K_m(n)\} \tag{11}$$

i.e., that $K_{i \cdot ITP}$ is larger than the corresponding $K_{m \cdot ATP}$ by a factor, R, which is constant for all modes of catalysis. Thus, in Eqn. 10, the term in the denominator for the apparent K_m simplifies to

$$K_A = K_m + ([ITP]/R) \tag{12}$$

and, for the nth mode of catalysis, will be referred to as $K_A(n)$. Thus, as shown in Theoretical treatment, the proportion of CF_1 with one site occupied by ATP is given by $H1$, where

$$H1 = [ATP]/([ATP] + K_A1) \tag{13}$$

and the proportion with one site occupied by ITP is given by $I1$, where

$$I1 = [ITP]/([ITP] + R\{K_m1 + [ATP]\}) \tag{14}$$

We assume cooperativity between the nucleotide binding sites, as above, and further assume that ITP binding to a catalytic site elicits the same cooperative interactions as would ATP binding. Thus, as in Eqn. 4, the proportion of CF_1 with its second site occupied by ATP (irrespective of whether the first is occupied by ATP or ITP) is given by $H2$, where

$$H2 = (H1 + I1)([ATP]/\{[ATP] + K_A2\}) \tag{15}$$

and the proportion with a second site occupied by ITP is given by $I2$, where

$$I2 = (H1 + I1)([ITP]/\{[ITP] + R(K_m2 + [ATP])\}) \tag{16}$$

Finally, the proportion of CF_1 with a third site occupied by ATP (irrespective of the nature of the nucleotides in sites 1 and 2) is given by $H3$, where

$$H3 = (H2 + I2)([ATP]/\{[ATP] + K_A3\}) \tag{17}$$

In the presence of ITP, the rate of ATP hydrolysis by each catalytic mode (denoted by $HV1$, $HV2$ or $HV3$) is found by multiplying the proportion of CF_1 with 1, 2 or 3 catalytic sites occupied by the corresponding values of V_{max}, and applying the 'suppression assumption' (cf. Eqns. 5, 6, 7). So,

$$HV1 = (H1 - H2)V_{max}1 \tag{18}$$

$$HV2 = (H2 - H3)V_{max}2 \tag{19}$$

$$HV3 = H3 \cdot V_{max}3 \tag{20}$$

and the overall rate, $HV6$, is the sum of these component rates:

$$HV6 = HV1 + HV2 + HV3 \tag{21}$$

Let the rate of ATP hydrolysis in the absence of ITP be v, as defined by Eqn. 7. As the specific radioactivity of $[\gamma^{-32}P]ATP$ is not diluted by the addition of ITP, the factor, $Q(I)$ is given by the simple ratio

$$Q(I) = \frac{\text{rate of } [^{32}P]P_i \text{ release with ITP present}}{\text{rate of } [^{32}P]P_i \text{ release without ITP}} = HV6/v \tag{22}$$

$Q(I)$ is thus a function of ATP and ITP concentrations. Using the values of K_m and V_{max} values for ATP hydrolysis alone (Table I), and estimating the value of R (see text), the variation of $Q(I)$ with [ATP] can be predicted and compared with the experimental points.

References

1 Futai, M., Noumi, T. and Maeda, M. (1989) Annu. Rev. Biochem. 58, 111–136.
2 Penefsky,H.S. and Cross,R.L. (1991) Adv. Enzymol. Rel. Areas Mol. Biol. 64, 173–214.
3 Cross, R.L., Grubmeyer, C. and Penefsky, H.S. (1982) J. Biol. Chem. 257, 12092–12100.
4 Penefsky, H.S. (1988) J. Biol. Chem. 263, 6020–6022.
5 Cunningham, D. and Cross, R.L. (1988) J. Biol. Chem. 263, 18850–18856.
6 Cross, R.L., Grubmeyer, C. and Penefsky, H.S. (1982) J. Biol. Chem. 257, 12101–12105.
7 Gresser, M.J., Myers, J.A. and Boyer, P.D. (1982) J. Biol. Chem. 257, 12030–12038.
8 Bullough, D.A., Verburg, J.G., Yoshida, M. and Allison, W.S. (1987) J. Biol. Chem. 262, 11675–11683.
9 Berden, J.A. Hartog, A.F. and Edel, C.M. (1991) Biochim. Biophys. Acta 1057, 151–156.
10 Leckband, D. and Hammes, G.G. (1987) Biochemistry 26, 2306–2312.
11 Hutton, R.L. and Boyer, P.D. (1979) J. Biol. Chem. 254, 9990–9993.
12 Kohlbrenner, W.E. and Boyer, P.D. (1983) J. Biol. Chem. 258, 10881–10886.
13 Wood, J.M., Wise, J.G., Senior, A.E., Futai, M. and Boyer, P.D. (1987) J. Biol. Chem. 262, 2180–2186.
14 Andralojc, P.J. and Harris, D.A. (1990) Biochim. Biophys. Acta 1016, 55–62.
15 Harris, D.A., Gomez-Fernandez, J.C., Klungsoyr, L. and Radda, G.K. (1978) Biochim. Biophys. Acta 504, 364–383.
16 Strotmann, H., Bickel-Sandkotter, S., Edelmann, K., Schlimme, E., Boos, K.S. and Lüstorff, J. (1977) in Structure and Function of Energy-Transducing Membranes (Van Dam, K. and Van Gelder, B.F., eds.), pp. 307–317, Elsevier/North-Holland, Amsterdam.
17 Andralojc, P.J. and Harris, D.A. (1988) FEBS Lett. 233, 403–407.
18 Patrie, W.J. and McCarty, R.E. (1984) J. Biol. Chem. 259, 11121–11128.
19 Penefsky, H.S. (1977) J. Biol. Chem. 252, 2891–2899.
20 Selman, B.R. and Durbin, R.D. (1978) Biochim. Biophys. Acta 502, 29–37.
21 Hurn, B.A.L. and Chantler, S.M. (1980) Methods Enzymol. 70, 104–135.
22 Bradford, M. (1976) Anal. Biochem. 72, 248–254.
23 Stevenson, G.T. and Dorrington, K.J. (1970) Biochem. J. 118, 703–712.
24 Xue, Z., Melese, T., Stempel, K.E., Reedy, T.J. and Boyer, P.D. (1988) J. Biol. Chem. 263, 16880–16885.
25 Reimer, S. and Selman, B.R. (1978) J. Biol. Chem. 253, 7249–7255.
26 Harris, D.A. (1989) Biochim. Biophys. Acta 974, 156–162.
27 Andralojc, P.J. (1990) Ph.D. Thesis, University of Leeds (UK).
28 Schuster, S.M., Gertschen, R.J. and Lardy, H.A. (1976) J. Biol. Chem. 251, 6705–6710.
29 Kasho, V.N. and Boyer, P.D. (1984) J. Bioenerg. Biomemb. 16, 407–419.
30 Guerrero, K.J., Ehler, L.L. and Boyer, P.D. (1990) FEBS Lett. 270, 187–190.
31 Fromme, P. and Gräber, P. (1989) FEBS Lett. 259, 33–36.
32 Fromme, P. and Gräber, P. (1990) Biochim. Biophys. Acta 1020, 187–194.
33 Nadanaciva, S. and Harris, D.A. (1990) in Current Research in Photosynthesis, Vol. 3 (Baltscheffsky, M., ed.), pp. 41–44, Kluwer, Dordrecht.
34 Wise, J.G., Latchney, L.R., Ferguson, A.M. and Senior, A.E. (1984) Biochemistry 23, 1426–1432.
35 Noumi, T. Maeda, M. and Futai, M. (1987) FEBS Lett. 213, 381–384.
36 Andralojc, P.J. and Harris, D.A. (1992) FEBS Lett. 310, 187–192.
37 Gromet-Elhanan, Z. and Avital, S. (1992) Biochim. Biophys. Acta 1102, 379–385.
38 Al-Shawi, M.K., Parsonage, D. and Senior, A.E. (1990) J. Biol. Chem. 265, 5595–5601.
39 Boyer, P.D. (1989) FASEB J. 3, 2164–2178.
40 Muneyuki, E., Yoshida, M., Bullough, D.A. and Allison, W.S. (1991) Biochim. Biophys. Acta 1058, 304–311.
41 Miwa, K., Ohtsubo, M., Denda, K., Hisabori, T., Date, T. and Yoshida, M. (1989) J. Biochem. 106, 679–683.
42 Harris, D.A. and Slater, E.C. (1975) Biochim. Biophys. Acta 387, 335–348.